ICES REPORT   11-31

October 2011

Numerical Simulations of Cloaking Problems using a DPG Method

by

L. Demkowicz and Jichun Li

The Institute for Computational Engineering and Sciences
The University of Texas at Austin
Austin, Texas 78712

Report Documentation Page

1. REPORT DATE **OCT 2011**	2. REPORT TYPE	3. DATES COVERED **00-00-2011 to 00-00-2011**
4. TITLE AND SUBTITLE **Numerical Simulations of Cloaking Problems using a DPG Method**		5a. CONTRACT NUMBER
		5b. GRANT NUMBER
		5c. PROGRAM ELEMENT NUMBER
6. AUTHOR(S)		5d. PROJECT NUMBER
		5e. TASK NUMBER
		5f. WORK UNIT NUMBER
7. PERFORMING ORGANIZATION NAME(S) AND ADDRESS(ES) **University of Texas at Austin,Institute for Computational Engineering and Sciences,Austin,TX,78712**		8. PERFORMING ORGANIZATION REPORT NUMBER
9. SPONSORING/MONITORING AGENCY NAME(S) AND ADDRESS(ES)		10. SPONSOR/MONITOR'S ACRONYM(S)
		11. SPONSOR/MONITOR'S REPORT NUMBER(S)

12. DISTRIBUTION/AVAILABILITY STATEMENT **Approved for public release; distribution unlimited**

13. SUPPLEMENTARY NOTES

14. ABSTRACT

The paper reviews the construction of cloaks for 2D acoustic or electromagnetic waves using the Piola transform, and shows how the transform leads to the construction of a quasi-optimal test norm for the Discontinuous Petrov-Galerkin (DPG) method with optimal test functions for this class of problems. Numerical experiments for cylindrical and square cloaks illustrate the discussed concepts and show that the DPG method is effective in cloak simulations.

15. SUBJECT TERMS

16. SECURITY CLASSIFICATION OF:			17. LIMITATION OF ABSTRACT	18. NUMBER OF PAGES	19a. NAME OF RESPONSIBLE PERSON
a. REPORT **unclassified**	b. ABSTRACT **unclassified**	c. THIS PAGE **unclassified**	**Same as Report (SAR)**	**20**	

NUMERICAL SIMULATIONS OF CLOAKING PROBLEMS USING A DPG METHOD

L. Demkowicz[a] [1] and Jichun Li[b] [2]

[a] Institute for Computational Engineering and Sciences
The University of Texas at Austin, Austin, TX 78712, USA
[b] Dept. of Mathematical Sciences
University of Nevada Las Vegas, Las Vegas, NV 89154-4020, USA

Abstract

The paper reviews the construction of cloaks for 2D acoustic or electromagnetic waves using the Piola transform, and shows how the transform leads to the construction of a quasi-optimal test norm for the Discontinuous Petrov-Galerkin (DPG) method with optimal test functions for this class of problems. Numerical experiments for cylindrical and square cloaks illustrate the discussed concepts and show that the DPG method is effective in cloak simulations.

Key words: Invisible cloak, Discontinuous Petrov Galerkin method, Maxwell's equations.

AMS subject classification: 65N30, 35L15, 78M10.

1 Introduction

We begin by reviewing shortly the concept of Piola transforms lying behind the construction of parametric finite elements forming the exact sequence (see [10], p. 34).

Piola transforms.   Let $\boldsymbol{x} = \boldsymbol{T}(\boldsymbol{\xi})$ be a smooth transformation of a domain $\Omega \subset \mathbb{R}^3$ onto a domain $D \subset \mathbb{R}^3$. The transformation defines a corresponding map between spaces $H^1(\Omega)$ and $H^1(D)$,

$$u(\boldsymbol{x}) = \hat{u}(\boldsymbol{\xi}) = \hat{u}(\boldsymbol{T}^{-1}(\boldsymbol{x})) = (\hat{u} \circ \boldsymbol{T}^{-1})(\boldsymbol{x}) \,. \tag{1.1}$$

The chain rule implies the corresponding transformation for gradients:

$$\frac{\partial u}{\partial x_i} = \frac{\partial \hat{u}}{\partial \xi_k} \frac{\partial \xi_k}{\partial x_i}.$$

If we want to preserve the exact sequence property, we need to transform the larger space $H(\mathbf{curl}, \Omega)$ using the same rule:

$$E_i = \hat{E}_k \frac{\partial \xi_k}{\partial x_i} \ . \tag{1.2}$$

In turn, for the curl operator we have:

$$\epsilon_{ijk} \frac{\partial E_k}{\partial x_j} = \epsilon_{ijk} \frac{\partial}{\partial x_j} \left(\hat{E}_l \frac{\partial \xi_l}{\partial x_k} \right) = \epsilon_{ijk} \frac{\partial \hat{E}_l}{\partial x_j} \frac{\partial \xi_l}{\partial x_k} + \hat{E}_l \underbrace{\epsilon_{ijk} \frac{\partial^2 \xi_l}{\partial x_k \partial x_j}}_{=0} = \epsilon_{ijk} \frac{\partial \hat{E}_l}{\partial \xi_m} \frac{\partial \xi_m}{\partial x_j} \frac{\partial \xi_l}{\partial x_k} \ , \tag{1.3}$$

where ϵ_{ijk} denotes the Rizzi symbol, i.e.,

$$\epsilon_{ijk} = \left\{ \begin{array}{cl} 0 & \text{if any two of indices ijk are equal,} \\ 1 & \text{if ijk is an even permutation of 123,} \\ -1 & \text{if ijk is an odd permutation of 123.} \end{array} \right.$$

But,

$$\epsilon_{ijk} \frac{\partial \xi_m}{\partial x_j} \frac{\partial \xi_l}{\partial x_k} = J^{-1} \epsilon_{nml} \frac{\partial x_i}{\partial \xi_n} \ ,$$

where J^{-1} is the inverse jacobian. Consequently, we obtain the following Piola transform for the curl operator:

$$\epsilon_{ijk} \frac{\partial E_k}{\partial x_j} = J^{-1} \frac{\partial x_i}{\partial \xi_n} \left(\epsilon_{nml} \frac{\partial \hat{E}_l}{\partial \xi_m} \right) \ . \tag{1.4}$$

This leads to the transform for the $H(\mathrm{div}, \Omega)$-conforming fields:

$$H_i = J^{-1} \frac{\partial x_i}{\partial \xi_n} \hat{H}_n \ . \tag{1.5}$$

Finally,

$$\frac{\partial H_i}{\partial x_i} = \underbrace{\frac{\partial}{\partial x_i} \left(J^{-1} \frac{\partial x_i}{\partial \xi_k} \right)}_{=0} \hat{H}_k + J^{-1} \frac{\partial x_i}{\partial \xi_k} \frac{\partial \hat{H}_k}{\partial \xi_l} \frac{\partial \xi_l}{\partial x_i} = J^{-1} \frac{\partial \hat{H}_k}{\partial \xi_k} \ , \tag{1.6}$$

which establishes the transformation rule for the L^2-conforming elements:

$$f = J^{-1} \hat{f} \ . \tag{1.7}$$

The Piola transforms set gradient into gradient, curl into curl and div into div. Consequently, any differential operator involving the grad, curl, and div operators preserves its structure at a possible expense of introducing an anisotropy in the "material data". In particular, the Piola transforms preserve the Maxwell equations and linear acoustics equations.

2

2D Maxwell and acoustics equations. Consider the Maxwell equations:

$$\begin{cases} \nabla \times \boldsymbol{E} + i\omega\mu\boldsymbol{H} &= 0, \\ \nabla \times \boldsymbol{H} - i\omega\epsilon\boldsymbol{E} &= 0, \end{cases} \tag{1.8}$$

where $\boldsymbol{E}$ and $\boldsymbol{H}$ are the electric and magnetic fields, and ϵ and μ are the permittivity and permeability, respectively. In the 2D transverse electric case, $\boldsymbol{E} = (E_1, E_2, 0)$ and $\boldsymbol{H} = (0, 0, H)$. Using a clockwise rotation by 90 degrees, we transform the 2D Maxwell equations into the 2D linear acoustics equations:

$$\begin{cases} i\omega\mu p + \mathrm{div}\,\boldsymbol{u} &= 0 \\ i\omega\epsilon\boldsymbol{u} + \nabla p &= \boldsymbol{0}, \end{cases} \tag{1.9}$$

where pressure $p = H$, and velocity $\boldsymbol{u} = (u_1, u_2) = (E_2, -E_1)$. Thus the 2D Maxwell and acoustics problems are equivalent, and any result established for one case immediately applies to the other case as well.

Construction of an invisible cloak for electromagnetic waves is based on introducing a singular bijective map $\boldsymbol{x} = \boldsymbol{x}(\boldsymbol{\xi})$ that maps a domain $\Omega - \{P\}$, where point $P \in \Omega$, onto a domain D with a hole, in such a way that the corresponding inverse map transforms the boundary of the hole into the single point P. Specific constructions for a cylindrical and square cloaks are discussed in the next section.

The linear acoustics equations with constant material data μ, ϵ in domain $\Omega - P$, transform then into acoustics equations in domain D with anisotropic material data:

$$\begin{cases} i\omega\hat{\mu}\hat{p} &+ \frac{\partial \hat{u}_k}{\partial \xi_k} &= 0 \\ i\omega\hat{\epsilon}_{ln}\hat{v}_n &+ \frac{\partial \hat{p}}{\partial \xi_l} &= 0, \end{cases} \tag{1.10}$$

where

$$\hat{\mu} = \mu J, \quad \hat{\epsilon}_{ln} = \epsilon \frac{\partial x_i}{\partial \xi_l} \frac{\partial x_i}{\partial \xi_n} J^{-1}. \tag{1.11}$$

The concept is illustrated in Fig. 1 showing the real part of pressure corresponding to a plane wave propagating horizontally, and the corresponding composition of the same function with the cylindrical cloaking map defined in Section 2. The map maps a hollow cylinder into the circular domain in such a way that the inner circle is mapped onto the origin. The rest of the domain remains intact. As a consequence of the construction, the plane wave remains unchanged outside of the cylinder but it is modified within its interior. The function on the right represents the solution to 2D acoustics or Maxwell equations with anisotropic material properties within the hollow cylinder (the cloak) implied by the singular map. The wave does not penetrate into the cloaked region (the inner circle) and remains unchanged outside.

2 Design of cloak materials

General speaking, there are several major approaches to render objects invisible. For example, Alu and Engheta [2] proposed to use plasmonic coatings to cancel the dipolar scattering. But this technique is limited to
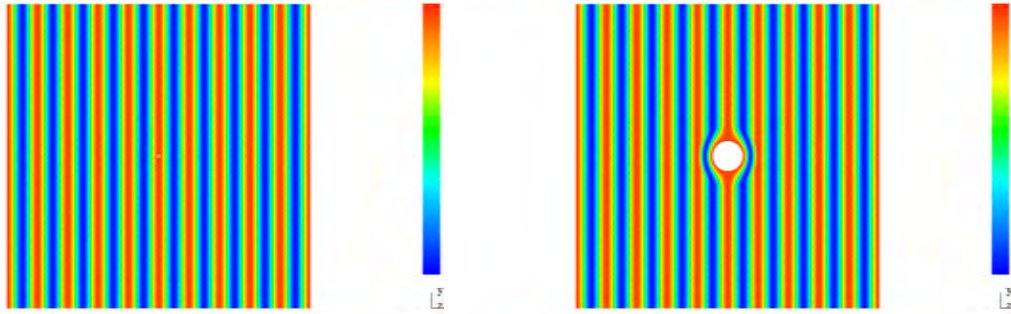
Figure 1: Cylindrical cloak in 2D. Left: $\mathrm{Re}(p(\boldsymbol{x}))$, right: $\mathrm{Re}(p(\boldsymbol{\xi}))$ with $p(\boldsymbol{x}) = e^{i\omega x_1}$ and cloaking map $\boldsymbol{x} = \boldsymbol{T}(\boldsymbol{\xi})$ from Section 2.

the sub-wavelength scale of the object, and the coating depends on the geometry and material parameters of the object. Milton and Nicorovici [17] discovered that using a metamaterial coating would cloak polarizable line dipoles. But the coating is affected by the objects placed inside. In 2006, Leonhardt [13] and Pendry *et al* [18] independently discovered a coordinate transformation mechanism for electromagnetic cloaking. Their mechanism was quite similar to that of Greenleaf *et al* [11, **?**] introduced for conductivity. The main idea is to design a special metamaterial to guide electromagnetic wave around the cloaked region. In May 2006, the first full wave numerical simulations on cylindrical cloaking was carried out by Cummer *et al* [5]. A few months later, the first experiment of such a cloak at microwave frequencies was successfully demonstrated by Schurig *et al* [20].

Since 2006, there have been many works devoted to a study of using metamaterials [14] to construct invisibility cloaks of different shapes (e.g., [12, 16, 19, 21, 22]). The fundamental idea is based on the principle discussed in the Introduction in context of 2D equations - the Maxwell equations are form invariant under coordinate transformations.

For simplicity, we shall consider only two cloak structures: a cylindrical cloak and a square cloak.

Cylindrical cloak. Following [18], a cylindrical region $r \leq R_1$ can be cloaked by a concentric cylindrical annulus $R_1 \leq r \leq R_2$ through the following coordinate transformation:

$$\begin{cases} r'(r,\theta) = \frac{R_2 - R_1}{R_2} r + R_1, & 0 \leq r \leq R_2, \\ \theta'(r,\theta) = \theta, & 0 \leq \theta \leq 2\pi, \end{cases} \qquad (2.12)$$

where the polar coordinate (r, θ) is related to the Cartesian coordinate (x, y) by

$$r = \sqrt{x^2 + y^2}, \quad \theta = \tan^{-1}\frac{y}{x}. \qquad (2.13)$$

Through some algebraic calculation (details can be seen in [15]), we can obtain the transformation

matrix

$$A = \left(\frac{\partial x_i'}{\partial x_j}\right) = \begin{pmatrix} \frac{R_2-R_1}{R_2} + \frac{R_1}{r}\sin^2\theta & -\frac{R_1}{r}\sin\theta\cos\theta & 0 \\ symmetric & \frac{R_2-R_1}{R_2} + \frac{R_1}{r}\cos^2\theta & 0 \\ 0 & 0 & 1 \end{pmatrix},$$ (2.14)

whose determinant equals

$$\det(A) = \frac{R_2-R_1}{R_2}\left(\frac{R_2-R_1}{R_2} + \frac{R_1}{r}\right) = \left(\frac{R_2-R_1}{R_2}\right)^2 \cdot \frac{r'}{r'-R_1}.$$ (2.15)

Furthermore, the relative permittivity in the transformed space can be obtained as

$$\epsilon' = \begin{pmatrix} \epsilon'_{xx} & \epsilon'_{xy} & 0 \\ \epsilon'_{yx} & \epsilon'_{yy} & 0 \\ 0 & 0 & \epsilon'_z \end{pmatrix},$$

where

$$\epsilon'_{xx} = \left[\left(\frac{R_2-R_1}{R_2}\right)^2 + \frac{R_1}{r}\left(2\frac{R_2-R_1}{R_2} + \frac{R_1}{r}\right)\sin^2\theta\right]/\det(A),$$

$$\epsilon'_{xy} = \epsilon'_{yx} = \left[-\frac{R_1}{r}\left(2\frac{R_2-R_1}{R_2} + \frac{R_1}{r}\right)\sin\theta\cos\theta\right]/\det(A),$$

$$\epsilon'_{yy} = \left[\left(\frac{R_2-R_1}{R_2}\right)^2 + \frac{R_1}{r}\left(2\frac{R_2-R_1}{R_2} + \frac{R_1}{r}\right)\cos^2\theta\right]/\det(A),$$

and $\epsilon'_z = 1/\det(A)$. The permeability μ' has the same as permittivity ϵ'.

Square cloak. The same idea as above can be used to design a square-shaped cloak with inner square width $2S_1$ and outer square width $2S_2$. It can be seen that the coordinate transformation [19]:

$$\begin{cases} x'(x,y) = x\frac{S_2-S_1}{S_2} + S_1 \\ y'(x,y) = y\left(\frac{S_2-S_1}{S_2} + \frac{S_1}{x}\right) \end{cases}$$

mapped the right triangle in the original space into the right-subdomain in the transformed space (see Fig.2).

It is easy to prove that the transformation matrix in this case is

$$A_r = \begin{pmatrix} \frac{S_2-S_1}{S_2} & 0 & 0 \\ -\frac{yS_1}{x^2} & \frac{S_2-S_1}{S_2} + \frac{S_1}{x} & 0 \\ 0 & 0 & 1 \end{pmatrix},$$ (2.16)

which has determinant

$$\det(A_r) = \frac{S_2-S_1}{S_2}\left(\frac{S_2-S_1}{S_2} + \frac{S_1}{x}\right).$$ (2.17)

The relative permittivity in the transformed space can be obtained as [15]:

$$\epsilon'_r = \begin{pmatrix} \left(\frac{S_2-S_1}{S_2}\right)^2 & -\frac{yS_1}{x^2}\cdot\frac{S_2-S_1}{S_2} & 0 \\ symmetric & \left(\frac{yS_1}{x^2}\right)^2 + \left(\frac{S_2-S_1}{S_2} + \frac{S_1}{x}\right)^2 & 0 \\ 0 & 0 & 1 \end{pmatrix}/\det(A_r).$$ (2.18)
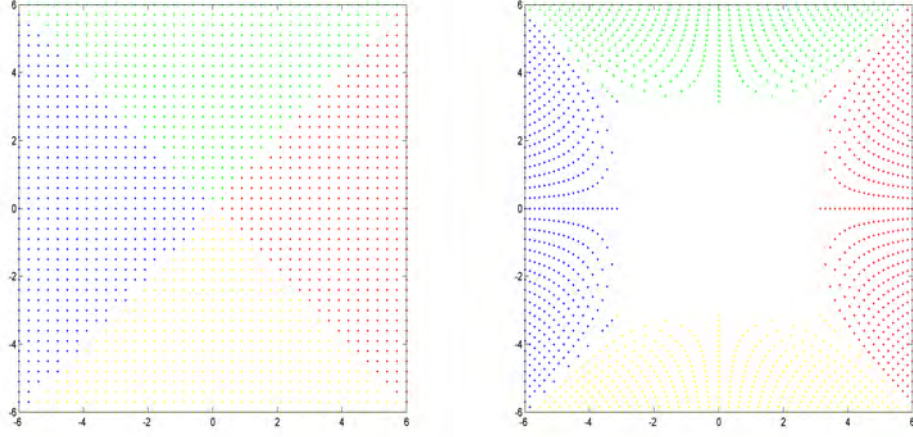
5

Figure 2: (Left) The original space; (Right) The transformed space.

Corresponding formulas for the upper, left and bottom triangles of the cloak can be similarly obtained by applying rotation matrix $R(\theta) = \begin{bmatrix} \cos\theta & -\sin\theta & 0 \\ \sin\theta & \cos\theta & 0 \\ 0 & 0 & 1 \end{bmatrix}$ to the right sub-domain with rotation angles $\theta = \pi/2, \pi$ and $3\pi/2$, respectively.

3 DPG Method

The *Discontinuous Petrov-Galerkin Method with Optimal Test Functions* [7, 23] builds on three crucial concepts:

- The idea of Petrov-Galerkin method with optimal test functions computed on the fly.

- The element-wise ultraweak variational formulation using discontinuous test functions that makes the determination of optimal test functions feasible.

- The choice of an optimal test norm that enables correct "mapping properties" and results in uniform stability for wave propagation, i.e., independent of the wavenumber.

For reader's convenience, here we review quickly these main points in context of linear acoustics, see [23, 8] for details.

Least squares and optimal testing. Any well-posed variational problem,

$$\begin{cases} u \in U \\ b(u,v) = l(v), \quad v \in V \end{cases} \tag{3.19}$$

6

with two Hilbert spaces U, V, sesquilinear form $b(u, v)$ and antilinear form $l(v)$, is equivalent to a linear operator problem,

$$Bu = l, \quad B : U \to V', \quad < Bu, v >_{V' \times V} = b(u, v). \tag{3.20}$$

What makes variational problems different from other linear problems is that the operator B takes values in the dual space V' equipped with the dual norm,

$$\|l\|_{V'} = \sup_{v \neq 0} \frac{|l(v)|}{\|v\|_V}. \tag{3.21}$$

Given a finite-dimensional subspace $U_h \subset U$, the least squares method seeks the minimizer of the quadratic minimum residual problem,

$$\frac{1}{2} \|Bu_h - l\|_{V'}^2 \to \min_{u_h \in U_h}. \tag{3.22}$$

Recalling the notion of the Riesz operator for test space V,

$$R_V : V \to V', \quad < R_V v, \delta v >= (v, \delta v)_V \tag{3.23}$$

and the fact that R_V is an isometry, we can reformulate the least squares problem as,

$$\frac{1}{2} \|R_V^{-1}(Bu_h - l)\|_V^2 \to \min_{u_h \in U_h}. \tag{3.24}$$

The corresponding necessary and equivalent[3] condition for the minimizer u_h takes form of the linear variational equation:

$$(R_V^{-1}(Bu_h - l), R_V^{-1} B\delta u_h)_V = 0, \quad \delta u_h \in U_h \tag{3.25}$$

or, recalling the definition of the Riesz operator,

$$< (Bu_h - l), R_V^{-1} B\delta u_h >= 0, \quad \delta u_h \in U_h. \tag{3.26}$$

Defining *trial-to-test operator* with the corresponding image identified as the *optimal test space* V_h,

$$U_h \ni \delta u_h \to v_h := R_V^{-1} B\delta u_h \in V_h \subset V, \tag{3.27}$$

we can reinterpret condition (3.26) as a Petrov-Galerkin method,

$$< (Bu_h - l), v_h >= 0, \quad R_V v_h = B\delta u_h, \tag{3.28}$$

or, returning to variational notation,

$$\begin{cases} u_h \in U_h \\ b(u_h, v_h) = l(v_h), \quad v_h \in V_h, \end{cases} \tag{3.29}$$

---

[3]Under the assumption of the well-posedness, the least squares quadratic functional is positive definite.

where the test functions are obtained by solving an auxiliary variational problem (inverting the Riesz operator R_V),

$$\begin{cases} v_h \in V_h \\ (v_h, \delta v)_V = b(\delta u_h, \delta v), \quad \delta v \in V_h. \end{cases} \tag{3.30}$$

The main points of the Petrov-Galerkin method are:

- The stiffness matrix is always hermitian and positive-definite.

- The method delivers the *best approximation error* (BAE) in the "energy norm":

$$\|u\|_E := \|Bu\|_{V'} = \sup_{v \in V} \frac{|b(u, v)|}{\|v\|_V}. \tag{3.31}$$

- The energy norm of the discretization error $u - u_h$ equals the residual and can be computed without knowing the exact solution,

$$\|u - u_h\|_E = \|Bu - Bu_h\|_{V'} = \|l - Bu_h\|_{V'} = \|R_V^{-1}(l - Bu_h)\|_V. \tag{3.32}$$

Hence, there is no need for a separate a-posteriori error estimation, the method comes with a built-in error estimator[4].

In fact, we do not have a single method but a family of such, any choice of test norm $\|v\|_V$ results in a different Petrov-Galerkin approximation. An obvious question to ask is how to select an optimal test norm. A possible answer comes from the Banach Closed Range Theorem. Under the assumption that the dual operator is injective, if we define the test norm as:

$$\|v\|_V := \sup_{u \in U} \frac{|b(u, v)|}{\|u\|_U}, \tag{3.33}$$

the corresponding energy norm coincides with the original norm in U,

$$\|u\|_E = \|u\|_U. \tag{3.34}$$

We deliver the best approximation error in the norm of our choice.

Ultraweak variational formulation and the DPG variational formulation. We review now the main ideas of the DPG method of C. Bottaso, P. Pausin, S. Micheletti, and R. Sacco [3, 4].

We solve the linear acoustics equations:

$$\begin{cases} i\omega \boldsymbol{u} + \nabla p &= \boldsymbol{0} \\ i\omega p + \operatorname{div}\boldsymbol{u} &= 0 \end{cases} \tag{3.35}$$

---

[4]Note the connection with implicit a-posteriori error estimation techniques aiming at element-wise approximation of inverse Riesz operator [1].

in a bounded domian Ω, accompanied by, e.g. hard boundary condition:

$$u_n = \boldsymbol{u} \cdot \boldsymbol{n} = g \text{ on } \Gamma = \partial\Omega. \tag{3.36}$$

We denote Ω_h for a disjoint partition of Ω into open elements K such as $\bar{\Omega} = \cup_{K \in \Omega_h} \bar{K}$, see Fig. 3.
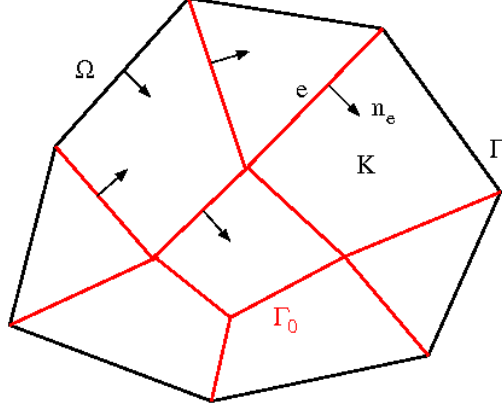

Figure 3: A FE mesh with elements K, edges e, skeleton Γ_h and internal skeleton Γ_h^0.

For any element K, multiplying the equations with test functions $\boldsymbol{v} \in \boldsymbol{H}(\mathrm{div}, K), q \in H^1(K)$ and integrating over the element K, we obtain

$$\begin{cases} i\omega \displaystyle\int_K \boldsymbol{u} \cdot \boldsymbol{v} + \int_K \nabla p \cdot \boldsymbol{v} & = 0 \\ i\omega \displaystyle\int_K p\, q + \int_K \mathrm{div}\boldsymbol{u}\, q & = 0. \end{cases} \tag{3.37}$$

We integrate by parts (relax) *both*[5] equations:

$$\begin{cases} i\omega \displaystyle\int_K \boldsymbol{u} \cdot \boldsymbol{v} - \int_K p \cdot \mathrm{div}\boldsymbol{v} + \int_{\partial K} p v_n & = 0 \\ i\omega \displaystyle\int_K p\, q - \int_K \boldsymbol{u} \cdot \nabla q + \int_{\partial K} u_n\, q\, \mathrm{sgn}(\boldsymbol{n}) & = 0, \end{cases} \tag{3.38}$$

where $u_n = \boldsymbol{u} \cdot \boldsymbol{n}_e$ and

$$\mathrm{sgn}(\boldsymbol{n}) = \begin{cases} 1 & \text{if } \boldsymbol{n} = \boldsymbol{n}_e \\ -1 & \text{if } \boldsymbol{n} = -\boldsymbol{n}_e. \end{cases} \tag{3.39}$$

Finally, contrary to the concept of numerical flux, we declare both traces and fluxes to be independent unknowns:

$$\begin{cases} i\omega \displaystyle\int_K \boldsymbol{u} \cdot \boldsymbol{v} - \int_K p \cdot \mathrm{div}\boldsymbol{v} + \int_{\partial K} \hat{p} v_n & = 0 \\ i\omega \displaystyle\int_K p\, q - \int_K \boldsymbol{u} \cdot \nabla q + \int_{\partial K} \hat{u}_n\, q\, \mathrm{sgn}(\boldsymbol{n}) & = 0. \end{cases} \tag{3.40}$$

---

[5]Hence the name of the ultra-weak variational formulation.

We use BCs to eliminate known fluxes

$$
\begin{cases}
i\omega \int_K \boldsymbol{u} \cdot \boldsymbol{v} - \int_K p \cdot \mathrm{div}\boldsymbol{v} + \int_{\partial K} \hat{p} v_n & = 0 \\
i\omega \int_K pq - \int_K \boldsymbol{u} \cdot \nabla q + \int_{\partial K - \Gamma} \hat{u}_n \, q \, \mathrm{sgn}(\boldsymbol{n}) & = \int_{\partial K \cap \Gamma} g \, q,
\end{cases} \tag{3.41}
$$

sum up over all elements, and introduce the standard DG notation:

$$
\begin{cases}
i\omega(\boldsymbol{u}, \boldsymbol{v})_{\Omega_h} - (p, \mathrm{div}\boldsymbol{v})_{\Omega_h} + < \hat{p}, v_n >_{\Gamma_h} & = 0 \\
i\omega(p, q)_{\Omega_h} - (\boldsymbol{u}, \nabla q)_{\Omega_h} + < \hat{u}_n, q >_{\Gamma_h^0} & = < g, q >_{\Gamma},
\end{cases} \tag{3.42}
$$

where we denote $(r, s)_{\Omega_h} := \sum_{K \in \Omega_h}(r, s)_K$, which reflects the element by element calculations. Furthermore, the precise functional setting is as follows:

$$
\begin{aligned}
\Gamma_h &:= \bigcup_K \partial K \quad \text{(skeleton)}, \\
\Gamma_h^0 &:= \Gamma_h - \partial\Omega \quad \text{(internal skeleton)}, \\
H^{1/2}(\Gamma_h) &:= \{q|_{\Gamma_h} \, : \, q \in H^1(\Omega)\} \text{ with the minimum extension norm:} \\
\|q\|_{H^{1/2}(\Gamma_h)} &:= \inf\{\|Q\|_{H^1} \, : \, Q|_{\Gamma_h} = q\}, \\
\widetilde{H}^{-1/2}(\Gamma_h^0) &:= \{v_n|_{\Gamma_h} \, : \, \boldsymbol{v} \in \boldsymbol{H}_0(\mathrm{div}, \Omega)\} \text{ with the minimum extension norm:} \\
\|v_n\|_{\widetilde{H}^{-1/2}(\Gamma_h^0)} &:= \inf\{\|\boldsymbol{v}\|_{\boldsymbol{H}_0(\mathrm{div}, \Omega)} \, : \, \boldsymbol{v} \cdot \boldsymbol{n}|_{\Gamma_h^0} = \sigma_n\}.
\end{aligned} \tag{3.43}
$$

We have two group variables:
Solution $\boldsymbol{U} = (\boldsymbol{u}, p, \hat{u}_n, \hat{p})$:

$$
\begin{aligned}
& u_1, u_2, p \in L^2(\Omega_h), \\
& \hat{u}_n \in \widetilde{H}^{-1/2}(\Gamma_h^0), \\
& \hat{p} \in H^{1/2}(\Gamma_h),
\end{aligned} \tag{3.44}
$$

and test function $\boldsymbol{V} = (\boldsymbol{v}, q)$:

$$
\begin{aligned}
& \boldsymbol{v} \in \boldsymbol{H}(\mathrm{div}, \Omega_h), \\
& q \in H^1(\Omega_h).
\end{aligned} \tag{3.45}
$$

The sesquilinear form can be written as:

$$
\begin{aligned}
b(\boldsymbol{U}, \boldsymbol{V}) &= -(\boldsymbol{u}, i\omega\boldsymbol{v} + \nabla q)_{\Omega_h} - (p, i\omega q + \mathrm{div}\boldsymbol{v})_{\Omega_h} \\
&\quad + < \hat{u}_n, q >_{\Gamma_h^0} + < \hat{p}, v_n >_{\Gamma_h}.
\end{aligned} \tag{3.46}
$$

There are two main punchlines:

- **Local invertibility of Riesz operator.** Due to the use of "broken" Sobolev spaces (discontinuous test functions), the Riesz operator is inverted elementwise. Given any trial shape functions, we compute the corresponding optimal test functions on the fly.

- **Approximate optimal test functions.** The locally determined optimal test functions still need to be approximated. This is done using standard Bubnov-Galerkin method and an *enriched space*. If polynomials of order p are used to approximate the unknown velocity and pressure, the approximate optimal test functions are determined using polynomials of order: $p + \Delta p$, where $\Delta p \geq 1$.

Requesting the L^2-norm for velocity $\boldsymbol{u}$ and pressure p, and some unknown (at this point yet) norms to define the minimum extension norms for traces and fluxes,

$$\|(\boldsymbol{u}, p, \hat{u}_n, \hat{p})\|_U^2 = \|\boldsymbol{u}\|_{L^2}^2 + \|p\|_{L^2}^2 + \|\hat{u}_n\|_?^2 + \|\hat{p}\|_?^2, \tag{3.47}$$

we can compute the optimal test norm (3.33):

$$
\begin{aligned}
\|(\boldsymbol{v}, q)\|_{opt}^2 \; &= \|i\omega\boldsymbol{v} + \nabla q\|_{\Omega_h}^2 + \|i\omega q + \mathrm{div}\boldsymbol{v}\|_{\Omega_h}^2 \\
&+ \sup_{\hat{u}_n, \hat{p}} \frac{|<\hat{u}_n, q> + <\hat{p}, v_n>|}{(\|\hat{u}_n\|_?^2 + \|\hat{p}_?^2)^{1/2}}.
\end{aligned}
\tag{3.48}
$$

The terms involving traces are unfortunately non-local[6], which makes the optimal test norm unsuitable for computations.

The following quasi-optimal test norm was proposed in [23, 8]:

$$\|(\boldsymbol{v}, q)\|_{opt}^2 = \|i\omega\boldsymbol{v} + \nabla q\|_{\Omega_h}^2 + \|i\omega q + \mathrm{div}\boldsymbol{v}\|_{\Omega_h}^2 + \|\boldsymbol{v}\|^2 + \|q\|^2, \tag{3.49}$$

where $\|\cdot\|$ denotes the L^2-norm on Ω. With the same norm used to define the minimum energy extension norms for traces and fluxes, it was shown[7] in [8] that the quasi-optimal test norm is equivalent to the optimal test norm *uniformly* in wave number k and mesh parameters: element size h and polynomial order p.

Consequently, we have the robust stability in the *desired norm*:

$$
\begin{aligned}
\left(\|\boldsymbol{u} - \boldsymbol{u}_h\|^2 + \|p - p_h\|^2 + \|\hat{u}_n - \hat{u}_{n,h}\|^2 + \|\hat{p} - \hat{p}_h\|^2\right)^{\frac{1}{2}} \\
\lesssim \|(\boldsymbol{u}, p, \hat{u}_n, \hat{p}) - (\boldsymbol{u}_h, p_h, \hat{u}_{n,h}, \hat{p}_h)\|_E \\
= \text{BAE of } (\boldsymbol{u}, p, \hat{u}_n, \hat{p}) \text{ in the energy norm} \\
\lesssim \text{BAE of } (\boldsymbol{u}, p, \hat{u}_n, \hat{p}) \text{ in the desired norm.}
\end{aligned}
\tag{3.50}
$$

The ultimate, pollution-free DPG method for wave propagation problems. Despite the uniform stability, the result above *does not* prove that DPG is a pollution free method in multidimensions. This is because the best approximation error term includes the best approximation error for traces and fluxes which is *not* pollution free. In 1D, fluxes and traces are just numbers, so their best approximation error (in any norm) is always zero.

---

[6]For regular functions, they can be interpreted as jumps in v_n and q on Γ_h.

[7]Under standard technical assumptions.

The method proposed and analyzed in [9] is a slight variation of the presented method, and it is obtained formally by rescaling the L^2-term in (3.49) with a small constant α,

$$\|(\boldsymbol{v}, q)\|_{opt}^2 = \|i\omega\boldsymbol{v} + \nabla q\|_{\Omega_h}^2 + \|i\omega q + \mathrm{div}\boldsymbol{v}\|_{\Omega_h}^2 + \alpha\left(\|\boldsymbol{v}\|^2 + \|q\|^2\right) \tag{3.51}$$

and passing with $\alpha \to 0$. The corresponding method *is pollution free*, see [9] for the proof. In practice, we use the test norm above with a small value of α limited by round off error only.

4 DPG Method for Cloaking Problems

We consider the 2D acoustics/Maxwell problem discussed in the previous section:

$$\begin{cases} i\omega\displaystyle\int_{\Omega_h}\boldsymbol{u}\cdot\boldsymbol{v} - \int_{\Omega_h}p\cdot\mathrm{div}\boldsymbol{v} + \int_{\partial\Omega_h}\hat{p}v_n &= 0 \\[2mm] i\omega\displaystyle\int_{\Omega_h}pq - \int_{\Omega_h}\boldsymbol{u}\cdot\nabla q + \int_{\partial\Omega_h-\Gamma}\hat{u}_n\,q\,\mathrm{sgn}(\boldsymbol{n}) &= \displaystyle\int_{\partial\Omega_h\cap\Gamma}g\,q. \end{cases} \tag{4.52}$$

The quasi-optimal test inner product discussed in Section 3 has the form:

$$\int_{\Omega_h}(i\omega\mu q + \mathrm{div}\boldsymbol{v})\overline{(i\omega\mu\delta q + \mathrm{div}\delta\boldsymbol{v})}d\boldsymbol{x} + \int_{\Omega_h}(i\omega\epsilon\boldsymbol{v} + \nabla q)\overline{(i\omega\epsilon\delta\boldsymbol{v} + \nabla\delta q)}d\boldsymbol{x} + \alpha\left(\int_{\Omega_h}\mu q\overline{\delta q}\,d\boldsymbol{x} + \int_{\Omega_h}\epsilon\boldsymbol{v}\overline{\delta\boldsymbol{v}}\,d\boldsymbol{x}\right). \tag{4.53}$$

As usual, the differential operators are understood elementwise (as indicated by integration over Ω_h). Note that we have used ϵ and μ to define the L^2 weighted norms.

The cloaking stretching $\boldsymbol{x} = \boldsymbol{x}(\boldsymbol{\xi})$ results in the test inner product in the $\boldsymbol{\xi}$ plane,

$$\int_{\widehat{\Omega}_h}(i\omega\hat{\mu}q + \widehat{\mathrm{div}}\hat{\boldsymbol{v}})\overline{(i\omega\hat{\mu}\delta q + \widehat{\mathrm{div}}\widehat{\delta\boldsymbol{v}})}\,J^{-1}d\boldsymbol{\xi} + \int_{\widehat{\Omega}_h}\frac{\partial\xi_k}{\partial x_i}\frac{\partial\xi_l}{\partial x_i}J(i\omega\hat{\epsilon}_{kn}\hat{v}_n + \frac{\partial\hat{q}}{\partial\xi_k})\overline{(i\omega\hat{\epsilon}_{lm}\widehat{\delta v}_m + \frac{\partial\widehat{\delta q}}{\partial\xi_l})}\,d\boldsymbol{\xi}$$

$$+\alpha\left(\int_{\widehat{\Omega}_h}\hat{\mu}\hat{q}\overline{\widehat{\delta q}}\,d\boldsymbol{\xi} + \int_{\widehat{\Omega}_h}\hat{\epsilon}_{nl}\hat{v}_n\overline{\widehat{\delta v}_l}\,d\boldsymbol{\xi}\right), \tag{4.54}$$

where

$$\hat{\mu} = \mu J, \quad \hat{\epsilon}_{nl} = \epsilon\frac{\partial x_i}{\partial\xi_n}\frac{\partial x_i}{\partial\xi_l}J^{-1}, \tag{4.55}$$

and also the *metric in the second term has changed* with the new metric tensor defined by:

$$\frac{\partial\xi_k}{\partial x_i}\frac{\partial\xi_l}{\partial x_i}J. \tag{4.56}$$

Thus, if we believe in the quasi-optimal test norm before the stretching, the formula above defines the right test norm to be used for the cloaking problem.

4.1 Basic Numerical Experiments

In this section, we will use our DPG method to solve two cloaking problems.

Cylindrical cloak   We use the following data:

wave number:	$k = 20.958$
domain:	$\Omega = (-1.5, 1.5)^2$
cloak dimensions:	$R_1 = 0.15, R_2 = 0.3$
material constants:	$\epsilon = 1, \mu = 1.$

Consistent with discussion in Section 2, we use the hard boundary condition along the inner radius of the cloak. Along the outer boundary of the domain, we use impedance boundary condition,

$$p - u_n = g \tag{4.57}$$

with data g driving the problem and determined using the very plane wave that we simulate. Impedance boundary condition (4.57) defines a relation between traces $\hat{p}$ and fluxes $\hat{u}_n$ on the exterior boundary Γ^{ext}. We have implemented it using Lagrange multipliers. More precisely, we enforce the following constraints on the unknown traces and fluxes,

$$\int_{\Gamma^{ext}} (p - u_n)\phi = \int_{\Gamma^{ext}} g\phi \tag{4.58}$$

for every test function ϕ coming from the flux space. With equal order of approximation for traces and fluxes being used in the simulations, the condition is equivalent to a pointwise condition,

$$p - u_n = P_h g \quad \text{on } \Gamma^{ext}, \tag{4.59}$$

where P_h is the L^2-projection on the flux space on Γ^{ext}.

We use the finite element mesh displayed in Fig. 4 with roughly four bilinear elements per wavelength. The color bar on the right-hand side represents order of H^1-conforming elements, in this case a uniform order $p = 2$. Consequently, the order of L^2-conforming elements [8] used to discretize "field variables": pressure p and velocity components u_1, u_2 is equal one (bilinear elements).

The shape of finite elements reflects transfinite parametrizations used to model the geometry (see [6] for details). Traces are discretized with continuous (and hence $H^{1/2}$-conforming) elements, and fluxes are approximated with quadratic discontinues elements. The optimal test functions are determined using the enriched space with $\Delta p = 2$. More precisely,

$$q, \delta q \in \mathcal{P}^{p+\Delta p} \otimes \mathcal{P}^{p+\Delta p}, \quad v, \delta v \in (\mathcal{P}^{p+\Delta p} \otimes \mathcal{P}^{p+\Delta p-1}) \times (\mathcal{P}^{p+\Delta p-1} \otimes \mathcal{P}^{p+\Delta p})$$

with $p = 2$ and $\Delta p = 2$. We have used $\alpha = 1.d - 5$. Using $\alpha = 1$ gives only slightly bigger L^2-errors.

The real part of the pressure, shown in Fig. 5, differs very little (in an eye-ball norm...) from the exact solution presented earlier in Fig. 1. The only visible distorsions are attributed to the use of non-affine elements and resulting non-polynomial shape functions that affect the best approximation error.

---

[8]The code supports the whole exact sequence, i.e. H^1-,$H(\text{curl})$-, $H(\text{div})$- and L^2-conforming elements, with the order dictated by the exact sequence for Nédélec's triangles and quads of the first type.
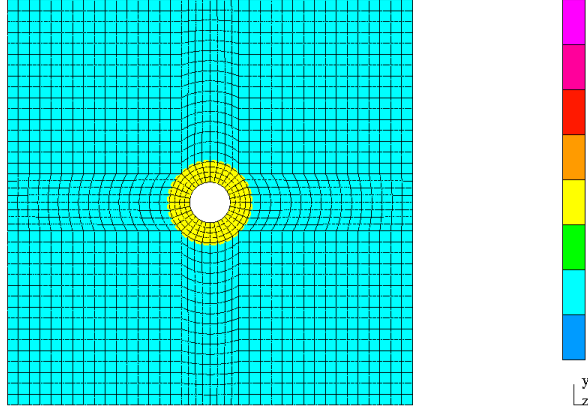
Figure 4: Cylindrical cloak in 2D: The FE mesh.

Square cloak.   We use the same data as for the cylindrical cloak:

wave number:	$k = 20.958$
domain:	$\Omega = (-1.5, 1.5)^2$
cloak dimensions:	$S_1 = 0.15, S_2 = 0.3$
material constants:	$\epsilon = 1, \mu = 1$.

We also use the same mesh with roughly four bilinear elements per wavelength. Fig.6 presents exact and approximate solutions for the problem. The relative L^2-error for the field variables $(\boldsymbol{u}, p)$ is 23.77 percent.

4.2   Experiments with h-Adaptivity

To reduce the relative errors, we further developed the h-adaptivity for our DPG method.

We first tested the "square cloak" problem to see how this works. Our initial mesh has rougly four bilinear elements per wavelength, and our h-adaptivity has produced essentially uniform refinements. The results show $O(h^2)$ convergence rate and the ratio of L^2 and energy errors stays bounded, which are consistent with our recent theoretical result [9]. Detailed results are presented in Table 1, where DOFs denote the total Degrees of Freedoms.

Similar results have been observed for the "cylindrical cloak" problem, details are presented in Table 2. The obtained optimal mesh after the fourth refinement is shown in Fig. 7. We also present the numerical and analytical solutions, and the error in Fig. 7.
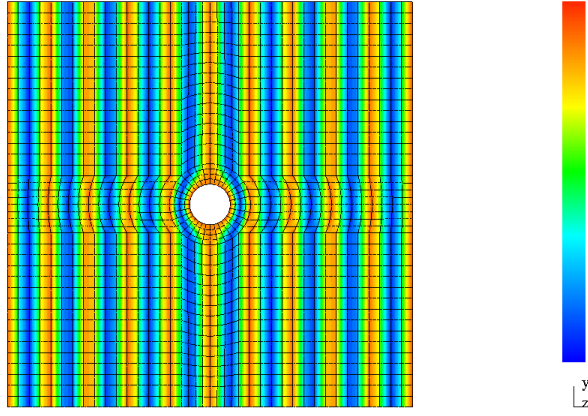
Figure 5: Cylindrical cloak in 2D: The real part of the computed pressure, range: (-1.22,1.31).

Table 1: The "square cloak": History of h-refinements.

Mesh	DOFs	Energy error	L2 error	L2 relative error (in %)	L2/energy error
1	2304	1.0922923104	0.3963140791	9.2788672579	0.3628278578
2	11064	0.3425376653	0.1002458536	2.3470467350	0.2926564398
3	45064	9.1168360988E-02	2.5464311229E-02	0.5961935165	0.2793108371
4	178512	2.3317027718E-02	6.6201235622E-03	0.1549963284	0.2839179865

4.3 Experiments with Pollution Errors

Finally, to demonstrate that our DPG method exhibits no dispersion error as proved in [9], we solved our cloak problems with different wave numbers and different mesh sizes (but keep kh fixed). Obtained numerical results are presented in Table 3, which clearly illustrates lack of pollution errors.

Table 2: The "cylindrical cloak": History of h-refinements.

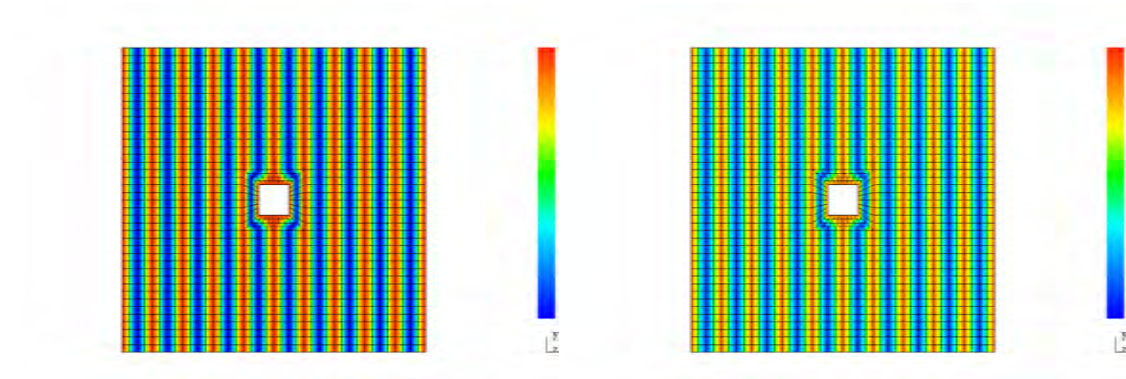| Mesh	DOFs	Energy error	L2 error	L2 relative error (in %)	L2/energy error
1	2304	1.4105574668	0.4205521701	9.8782505902	0.2981460734
2	9348	0.4918732768	0.1359146653	3.1924660088	0.2763204910
3	12572	0.4434205623	0.1076659299	2.5289206723	0.2428077068
4	14282	0.3988570480	0.1057855040	2.4848211457	0.2652215990

Figure 6: Cylindrical cloak in 2D: The real part of computed pressure. Left: the exact solution, range: (-1,1); Right: the approximate one, range: (-1.24,1.29).

Table 3: Experiments with pollution errors for both cloaking problems.

		square cloak	cylindrical cloak
Wavenumbers	DOFs	L2 relative error (in %)	L2 relative error (in %)
0.52396E+01	4800	9.27887	9.87825
0.10479E+02	18960	9.32685	9.68599
0.20958E+02	75360	9.39416	10.07621
0.41917E+02	300480	9.49858	10.19268

5 Conclusions

In this paper we extend our recently developed Discontinuous Galerkin Method (DPG) to the cloaking problems. Extensive numerical experiments demonstrate that the DPG method is indeed free of pollution error and quite efficient in solving this type of problems.
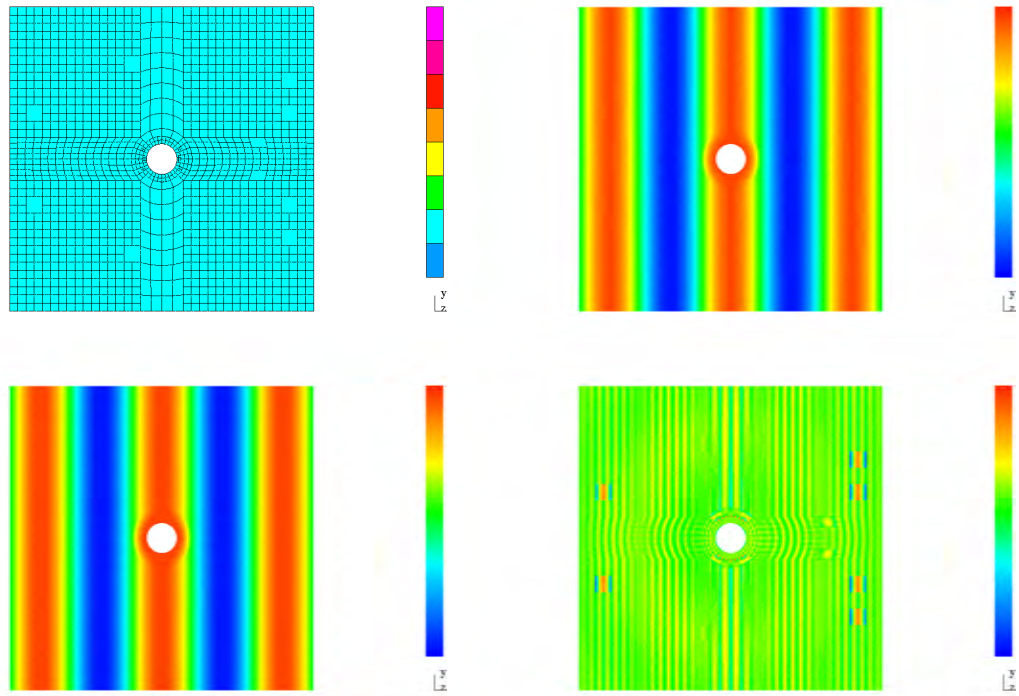
Figure 7: Cylindrical cloak after 4 refinements. Top Left: The mesh; Top Right: The real part of computed pressure, range: (-1.01, 1.05); Bottom Left: the exact solution, range: (-1,1); Bottom Right: the error approximate one, range: (-0.057,0.037).

References

[1] M. Ainsworth and J.T. Oden. *A Posteriori Error Estimation in Finite Element Analysis*. Wiley and Sons, Inc., New York, 2000.

[2] A. Alu and N. Engheta, Achieving transparency with plasmonic and metamaterial coatings, *Phys. Rev. E* 72, 016623 (2005).

[3] C.L. Bottasso, S. Micheletti, and R. Sacco. The discontinuous Petrov-Galerkin method for elliptic problems. *Comput. Methods Appl. Mech. Engrg.*, 191 (2002) 3391–3409.

[4] C.L. Bottasso, S. Micheletti, and R. Sacco. A multiscale formulation of the discontinuous Petrov-Galerkin method for advective-diffusive problems. *Comput. Methods Appl. Mech. Engrg.*, 194 (2005) 2819–2838.

[5] S.A. Cummer, B.-I. Popa, D. Schurig, D.R. Smith and J. Pendry, Full-wave simulations of electromagnetic cloaking structures, *Physical Review E* 74, 036621 (2006).

[6] L. Demkowicz. *Computing with hp Finite Elements. I.One- and Two-Dimensional Elliptic and Maxwell Problems*. Chapman & Hall/CRC Press, Taylor and Francis, October 2006.

[7] L. Demkowicz and J. Gopalakrishnan. A class of discontinuous Petrov-Galerkin methods. Part II: Optimal test functions. *Numer. Meth. for PDEs*,27 (2011) 70–105. see also ICES Report 2009/16.

[8] L. Demkowicz, J. Gopalakrishnan, I. Muga, and J. Zitelli. Wavenumber explicit analysis for a DPG method for the multidimensional Helmholtz equation. Technical report, ICES, 2011-24.

[9] L. Demkowicz, J. Gopalakrishnan, I. Muga, and D. Pardo A DPG method for the multidimensional Helmholtz equation with no pollution. Technical report, ICES. in preparation.

[10] L. Demkowicz, J. Kurtz, D. Pardo, M. Paszyński, W. Rachowicz, and A. Zdunek. *Computing with hp Finite Elements. II. Frontiers: Three-Dimensional Elliptic and Maxwell Problems with Applications*. Chapman & Hall/CRC, October 2007.

[11] A. Greenleaf, Y. Kurylev, M. Lassas and G. Uhlmann, Cloaking devices, electromagnetics wormholes and transformation optics, *SIAM Review* 51 (2009) 3-33.

[12] R.V. Kohn, D. Onofrei, M.S. Vogelius and M.I. Weinstein, Cloaking via change of variables for the Helmholtz equation, *Comm. Pure Appl. Math.*, 63 (2010) 0973-1016.

[13] U. Leonhardt, Optical conformal mapping, *Science* 312 (2006) 1777-1780.

[14] J. Li, Numerical convergence and physical fidelity analysis for Maxwell's equations in metamaterials, *Comput. Methods Appl. Mech. Engrg.*, 198 (2009) 3161–3172.

[15] J. Li and Y. Huang, Mathematical simulation of cloaking metamaterial structures, *Advances in Applied Mathematics and Mechanics* (in review).

[16] G.W. Milton, M. Briane and J.R. Willis, On cloaking for elasticity and physical equations with a transformation invariant form, *New Journal of Physics*, 8 (2006) 248.

[17] G.W. Milton and N.P. Nicorovici, On the cloaking effects associated with anomalous localized resonance, *Proc. R. Soc. A*, 462 (2006) 3027-3059.

[18] J.B. Pendry, D. Schurig and D.R. Smith, Controlling electromagnetic fields, *Science*, 312 (2006) 1780-1782.

[19] M. Rahm, D. Schurig, D.A. Roberts, S.A. Cummer, D.R. Smith and J.B. Pendry, Design of electromagnetic cloaks and concentrations using form-invariant coordinate transformations of Maxwell's equations, *Photonics and Nanostructures - Fundamentals and Applications*, 6 (2008) 87-95.

[20] D. Schurig, J.J. Mock, B.J. Justice, S.A. Cummer, J.B. Pendry, A.F.S. Starr and D.R. Smith, Metamaterial Electromagnetic Cloak at Microwave Frequencies, *Science*, 314 (2006) 977-980.

[21] J. Zhang, J. Huangfu, Y. Luo, H. Chen, J.A. Kong and B.-I. Wu, Cloak for multilayered and gradually changing media, *Physical Review B* 77, 035116 (2008).

[22] Y. Zhao and Y. Hao, Full-wave parallel dispersive finite-difference time-domain modeling of three-dimensional electromagnetic cloaking structures, *J. Comp. Phys.*, 228 (2009) 7300-7312.

[23] J. Zitelli, I. Muga, L. Demkowicz, J. Gopalakrishnan, D. Pardo and V. Calo, A class of discontinuous Petrov-Galerkin methods. Part IV: Wave propagation problems. *J. Comp. Phys.*, 230 (2011) 2406-2432. see also ICES Report 2010/17.